JACC: CARDIOONCOLOGY VOL. 6, NO. 2, 2024
© 2024 THE AUTHORS. PUBLISHED BY ELSEVIER ON BEHALF OF THE AMERICAN COLLEGE OF CARDIOLOGY FOUNDATION. THIS IS AN OPEN ACCESS ARTICLE UNDER THE CC BY-NC-ND LICENSE (http://creativecommons.org/licenses/by-nc-nd/4.0/).

MINI-FOCUS ISSUE: ANTHRACYCLINES

ORIGINAL RESEARCH

Anthracycline Cardiotoxicity Induces Progressive Changes in Myocardial Metabolism and Mitochondrial Quality Control

Novel Therapeutic Target

Anabel Díaz-Guerra, MSc,[a,b] Rocío Villena-Gutiérrez, PhD,[a] Agustín Clemente-Moragón, PhD,[a,b] Mónica Gómez, Tech,[a,c] Eduardo Oliver, PhD,[a,b,d] Miguel Fernández-Tocino, MSc,[a,b] Carlos Galán-Arriola, DVM, PhD,[a,b] Laura Cádiz, PhD,[a] Borja Ibáñez, MD, PhD[a,b,e]

ABSTRACT

BACKGROUND Anthracycline-induced cardiotoxicity (AIC) debilitates quality of life in cancer survivors. Serial characterizations are lacking of the molecular processes occurring with AIC.

OBJECTIVES The aim of this study was to characterize AIC progression in a mouse model from early (subclinical) to advanced heart failure stages, with an emphasis on cardiac metabolism and mitochondrial structure and function.

METHODS CD1 mice received 5 weekly intraperitoneal doxorubicin injections (5 mg/kg) and were followed by serial echocardiography for 15 weeks. At 1, 9, and 15 weeks after the doxorubicin injections, mice underwent fluorodeoxyglucose positron emission tomography, and hearts were extracted for microscopy and molecular analysis.

RESULTS Cardiac atrophy was evident at 1 week post-doxorubicin (left ventricular [LV] mass 117 ± 26 mg vs 97 ± 25 mg at baseline and 1 week, respectively; $P < 0.001$). Cardiac mass nadir was observed at week 3 post-doxorubicin (79 ± 16 mg; $P = 0.002$ vs baseline), remaining unchanged thereafter. Histology confirmed significantly reduced cardiomyocyte area (167 ± 19 μm^2 in doxorubicin-treated mice vs 211 ± 26 μm^2 in controls; $P = 0.004$). LV ejection fraction declined from week 6 post-doxorubicin (49% ± 9% vs 61% ± 9% at baseline; $P < 0.001$) until the end of follow-up at 15 weeks (43% ± 8%; $P < 0.001$ vs baseline). At 1 week post-doxorubicin, when LV ejection fraction remained normal, reduced cardiac metabolism was evident from down-regulated markers of fatty acid oxidation and glycolysis. Metabolic impairment continued to the end of follow-up in parallel with reduced mitochondrial adenosine triphosphate production. A transient early up-regulation of nutrient-sensing and mitophagy markers were observed, which was associated with mitochondrial enlargement. Later stages, when mitophagy was exhausted, were characterized by overt mitochondrial fragmentation.

CONCLUSIONS Cardiac atrophy, global hypometabolism, early transient-enhanced mitophagy, biogenesis, and nutrient sensing constitute candidate targets for AIC prevention. (J Am Coll Cardiol CardioOnc 2024;6:217–232) © 2024 The Authors. Published by Elsevier on behalf of the American College of Cardiology Foundation. This is an open access article under the CC BY-NC-ND license (http://creativecommons.org/licenses/by-nc-nd/4.0/).

From the [a]Centro Nacional de Investigaciones Cardiovasculares, Madrid, Spain; [b]Centro de Investigación Biomédica en Red de Enfermedades Cardiovasculares, Madrid, Spain; [c]Centro Nacional de Investigaciones Oncológicas, Madrid, Spain; [d]Centro de Investigaciones Biológicas Margarita Salas, Madrid, Spain; and the [e]Cardiology Department, IIS-Fundación Jiménez Díaz Hospital, Madrid, Spain.

ISSN 2666-0873 https://doi.org/10.1016/j.jaccao.2024.02.005

JACC: CARDIOONCOLOGY, VOL. 6, NO. 2, 2024
APRIL 2024:217–232

ABBREVIATIONS AND ACRONYMS

AIC = anthracycline-induced cardiotoxicity

AMPK = adenosine monophosphate–activated protein kinase

ATP = adenosine triphosphate

CT = computed tomography

FA = fatty acid

FDG = fluorodeoxyglucose

HF = heart failure

LV = left ventricle/ventricular

LVEF = left ventricular ejection fraction

OXPHOS = oxidative phosphorylation

PET = positron emission tomographic

TUNEL = terminal deoxynucleotidyl transferase dUTP nick-end labeling

Anthracyclines such as doxorubicin are among the most effective anticancer drugs and remain the first-line therapy (alone or in combination) for many cancer types.[1] However, anthracyclines are associated with irreversible damage to the myocardium, known as anthracycline-induced cardiotoxicity (AIC).[2] Up to 5% of cancer survivors treated with anthracyclines go on to develop chronic heart failure (HF) as a consequence of AIC.[3,4] Although AIC had been known for decades, there is a lack of specific therapies that can prevent this frequent secondary effect.[5,6]

The heart consumes more energy per unit weight than any other body organ, and to meet this intense energy demand, more than 30% of cardiomyocyte volume is occupied by mitochondria, enabling the production of large amounts of adenosine triphosphate (ATP) to support cardiac contraction. AIC involves a plethora of intermediate mechanisms that converge on the dysregulation of mitochondrial function.[7] Mitochondrial function and cardiomyocyte metabolism are both central to AIC, but there is a lack of comprehensive longitudinal studies evaluating key molecular players involved in these processes. Several studies have shown that doxorubicin irreversibly binds to cardiolipin in the inner mitochondrial membrane. The resulting disruption of the electron transport chain leads to an increase in the production of reactive oxygen species.[8] Doxorubicin has also been reported to induce defects in mitochondrial biogenesis[9] and an imbalance in mitochondrial dynamics.[10] Several studies have shown that AIC reduces fatty acid (FA) oxidation; however, the temporal association among FA oxidation impairment, mitochondrial dysfunction, and cardiac dysfunction during AIC is not well established, and it therefore remains unresolved whether FA oxidation impairment is a cause or consequence of mitochondrial dysfunction. The impact of doxorubicin on cardiomyocyte glycolysis is less clear, with some studies showing a compensatory up-regulation of glycolytic ATP production[11] and others reporting a down-regulation.[12] Most reports of these changes were cross-sectional and examined different stages in the development of AIC (most often after the appearance of overt cardiac dysfunction). Given that AIC is a dynamic process, there is a clear need to assess how mitochondrial function and cardiomyocyte metabolism change across different disease stages to identify potential therapeutic targets. In the present study, we examined these molecular changes in concert with cardiac imaging in a mouse model of AIC characterized by slow progression to cardiac dysfunction. We also specifically focused on male mice, given the potential differences according to sex in AIC.

METHODS

To mimic a clinical scenario of a progressively increasing cumulative anthracycline dose, adult male CD1 mice were given 5 weekly intraperitoneal injections of doxorubicin hydrochloride 2 mg/mL (#999958.2, Meiji Pharma; 5 mg/kg, resulting in a 25 mg/kg cumulative dose). Echocardiography was performed at baseline (before the first doxorubicin injection) and at 1, 3, 6, 9, 12, and 15 weeks after the final injection. Selected animals were sacrificed and hearts and blood collected for microscopy and molecular analysis at an early stage of modeled AIC (1 week after completion of the doxorubicin treatment regime), at an intermediate disease stage (9 weeks postinjection), and at an advanced disease stage (15 weeks postinjection). Combined positron emission tomographic (PET) and computed tomographic (CT) analysis of cardiac ^{18}F-fluorodeoxyglucose (FDG) uptake was conducted in animals at baseline and at the early, intermediate, and advanced AIC stages (**Figure 1**). Details of all methodologic procedures are provided in the Supplemental Methods.

The project was approved by the Institutional Animal Research Committee and conducted in accordance with the recommendations of the National Research Council Guide for the Care and Use of Laboratory Animals.

Transthoracic echocardiography was performed using a Vevo 2100 ultrasound system (Visual Sonics). PET/CT studies were performed using a small-animal PET/CT scanner (nanoScan, Mediso).

The authors attest they are in compliance with human studies committees and animal welfare regulations of the authors' institutions and Food and Drug Administration guidelines, including patient consent where appropriate. For more information, visit the Author Center.

Manuscript received September 11, 2023; revised manuscript received January 31, 2024, accepted February 6, 2024.

FIGURE 1 Study Design

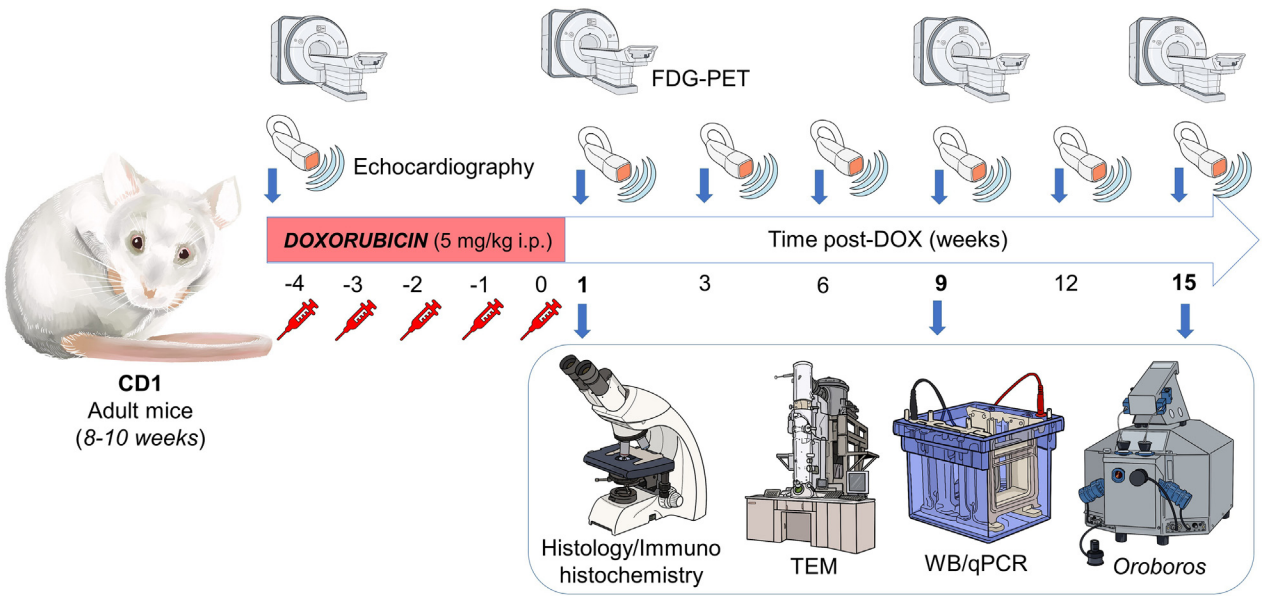

Male CD1 mice (8-10 weeks old) were randomly assigned to receive once weekly intraperitoneal injections of 5 mg/kg doxorubicin (DOX) for 5 weeks or no treatment (control). Echocardiographic examinations were performed at baseline (before the first injection) and 1, 3, 6, 9, 12, and 15 weeks after the end of the DOX treatment. Positron emission tomographic (PET)/computed tomographic scans were performed at baseline and 1, 9, and 15 weeks after DOX treatment. At 1, 9, and 15 weeks after DOX treatment, selected animals were sacrificed, and hearts were collected for further analysis by histology and immunohistochemistry, transmission electron microscopy (TEM), western blotting (WB), reverse transcriptase quantitative polymerase chain reaction (qPCR), and high-resolution mitochondrial respirometry (Oroboros Instruments). Syringe symbols indicate DOX injections. Arrows indicate defined time points. FDG = fluorodeoxyglucose.

STATISTICAL ANALYSIS. Data are presented as mean ± SD and were analyzed using Prism version 9.5.1 (GraphPad Software). Sample size was calculated using power analysis. A total of 258 animals were used (doxorubicin group, n = 157; no-treatment control group, n = 101). Data distributions were validated using the Shapiro-Wilk normality test. Two groups were compared using an unpaired Student's *t*-test or the Mann-Whitney *U* test according to data distribution. Comparisons among >2 groups were done using analysis of variance with Dunnett's or Šídák's post hoc test for multiple pairwise comparisons. Survival data were compared using a log-rank (Mantel-Cox) test. To compare longitudinal data, 1- or 2-way repeated-measures analysis of variance was used.

Detailed information on ex vivo methodologies can be found in the Supplemental Methods.

RESULTS

SYSTEMIC EFFECTS OF DOXORUBICIN TREATMENT. The survival rate for doxorubicin-treated mice was significantly lower than that for controls (**Figures 2A and 2B**), with a median survival time of 55 days among doxorubicin-treated mice. Body weight remained unaltered during the doxorubicin injection protocol, but mice began to lose weight from fifth injection onward (**Figure 2C**). In the early phase of AIC (1 week after the final doxorubicin injection), treated animals showed increased food intake (**Figure 2D**) and decreased basal activity (**Figure 2E**), both of which normalized with time. No changes were found in light-cycle energy expenditure (**Figure 2F**). At the intermediate stage of the disease, with subtle AIC, animals saw an elevated dark-cycle energy expenditure (**Figure 2G**).

Plasma glucose in fed or after 16 hours of fasting doxorubicin-exposed mice at the early disease stage was lower than in controls (Supplemental Figure 1A). Glucose tolerance testing showed normal insulin function during early AIC (Supplemental Figure 1B). Moreover, a reduction in plasma glucose levels was also seen at all disease stages analyzed (Supplemental Figure 1C). Plasma lactate and total plasma protein concentration were also both decreased in doxorubicin-treated mice at all disease stages (Supplemental Figures 1D and 1E). No similar consistent plasma changes were seen for ketone

FIGURE 2 Survival and Metabolic Activity

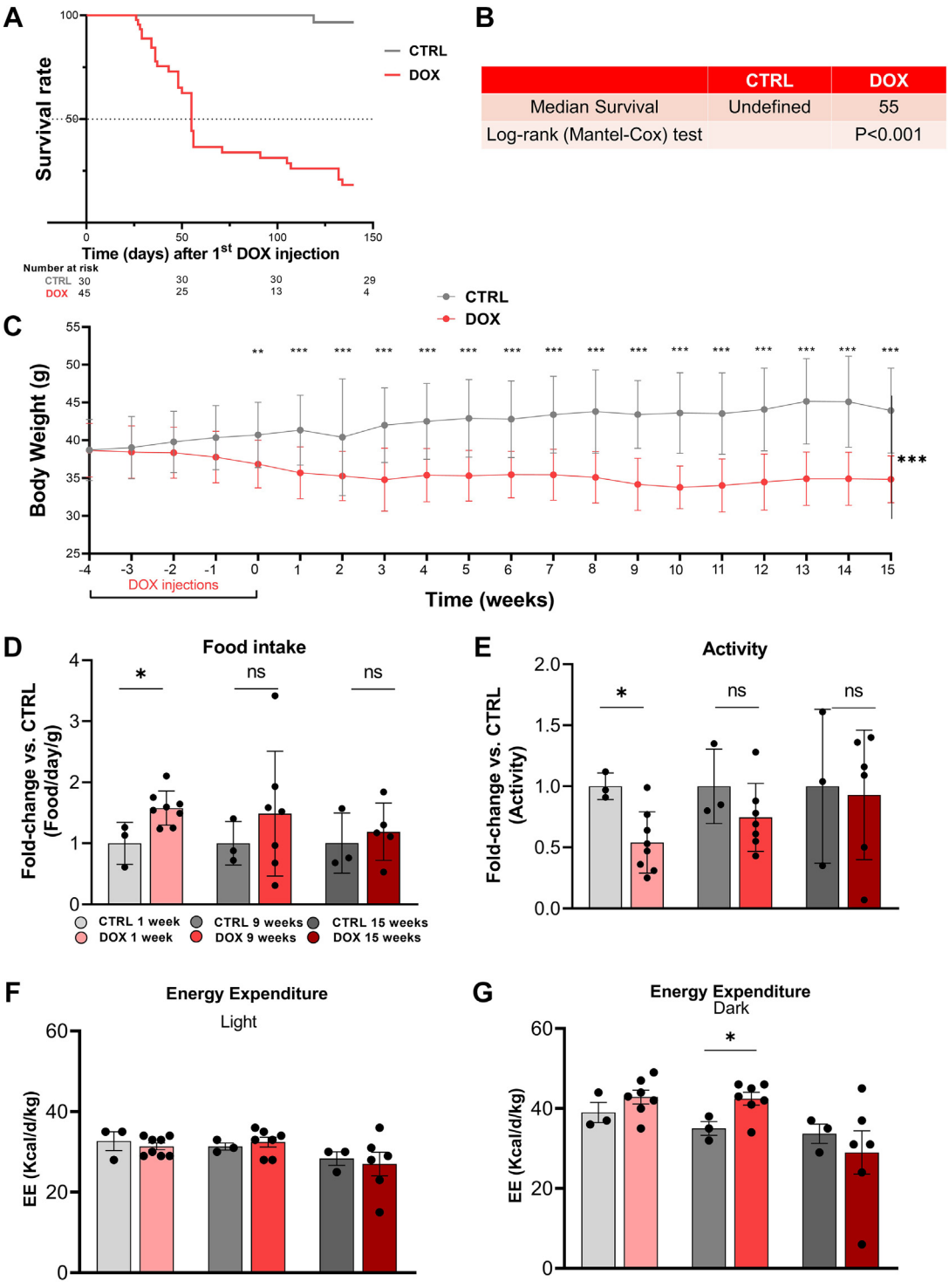

(A) Life span of mice after the first doxorubicin (DOX) injection. (B) Median survival (n = 30-45). The study was performed from the first DOX injection to 140 days (15 weeks post-DOX). (C) Body weight in mice (n = 9-50). (D) Food intake in mice 1, 9, and 15 weeks after DOX treatment and in time-paired controls (CTRL) (n = 3-8), presented as grams per day per body weight (g). (E) Physical activity analyzed in the same mouse groups as in (D) (n = 3-8). (F) Energy expenditure (EE) during light hours, analyzed in the same mouse groups as in (D), presented as kilocalories expended per day per body weight (g) (n = 3-8). (G) EE during dark hours, analyzed in the same mouse groups as in (D), presented as kilocalories expended per day per body weight (g) (n = 3-7). Data are presented as mean ± SD. Data were compared using unpaired Student's *t*-test, Mann-Whitney *U* test, 2-way repeated-measures analysis of variance with Šídák's post hoc test multiple comparison, or log-rank test. $^{*}P < 0.05$, $^{**}P < 0.01$, and $^{***}P < 0.001$.

bodies, nonesterified FAs, or lipase (Supplemental Figures 1F-1H).

DOXORUBICIN TREATMENT TRIGGERS CARDIOMYOCYTE ATROPHY AND AN EARLY REDUCTION IN CARDIAC MASS. In early-stage AIC (1 week post-doxorubicin), left ventricular (LV) mass was significantly reduced (117 ± 26 mg vs 97 ± 25 mg at baseline and 1 week, respectively; $P < 0.001$). LV mass continued to decrease until the end of the study (70 ± 9 mg at 15 weeks; $P < 0.001$ vs baseline) (**Figure 3A**). LV mass remained unchanged in control mice during the study period (**Figure 3B**).

Heart weight/tibia length ratio in doxorubicin-treated mice was significantly lower than in controls in early AIC (at 1 week post-doxorubicin, 8.45 ± 1.79 mg/mm vs 11.51 ± 1.62 mg/mm in controls; $P = 0.001$) and in advanced AIC (at 15 weeks post-doxorubicin, 8.21 ± 1.71 mg/mm; $P < 0.001$ vs control) (**Figure 3C**). Heart weight reduction was accompanied by a decrease in cardiomyocyte area both in early AIC (at 1 week post-doxorubicin, 167 ± 19 μm^2 vs 211 ± 26 μm^2 in controls; $P = 0.004$) and in advanced AIC (at 15 weeks post-doxorubicin, 176 ± 14 μm^2; $P = 0.0203$ vs control) (**Figures 3D and 3E**). Cardiac atrophy was accompanied by an increase in DNA damage, indexed as the number of terminal deoxynucleotidyl transferase dUTP nick-end labeling (TUNEL)-positive cardiac cells (**Figures 3F and 3G**). Doxorubicin-treated mice also showed more pronounced and extensive cardiac fibrosis at 15 weeks post-doxorubicin (**Figures 3H and 3I**).

DOXORUBICIN TREATMENT IS ASSOCIATED WITH SLOW-PROGRESSING LV SYSTOLIC DYSFUNCTION. Serial echocardiography revealed a progressive decline in LV ejection fraction (LVEF) after doxorubicin treatment, with the decline becoming significant at week 6 (61% ± 9% vs 49% ± 9% at baseline and 6 weeks, respectively; $P < 0.001$) (**Figures 4A and 4B**). LVEF reached its lowest value at 15 weeks after doxorubicin treatment (43% ± 8%; $P < 0.001$ vs baseline). LVEF remained unchanged in control mice during the study period (**Figure 4C**). The rest of the echocardiographic parameters are shown in Supplemental Table 1. A similar decline in LVEF was observed in mice treated with doxorubicin by intravenous injection over the same time scale; however, intravenous administration was associated with a higher mortality rate (data not shown).

DOXORUBICIN TREATMENT REDUCES GLOBAL CARDIAC METABOLISM. Reverse transcriptase quantitative polymerase chain reaction analysis of cardiac tissue for genes encoding proteins involved in FA metabolism and mitochondrial FA import revealed a general down-regulation as early as 1 week after the end of doxorubicin treatment, before the detection of reduced cardiac systolic function. This down-regulation affected all markers of metabolic pathways examined: carnitine palmitoyl transferase 1A and 2 (*Cpt1a* and *Cpt2*), acyl-coenzyme A thioesterase 1 (*Acot1*), peroxisomal acyl-coenzyme A oxidase 1 (*Acox1*), carnitine O-acetyltransferase (*Crat*), and lipase E (*Lipe*). At the advanced disease stage (15 weeks post-doxorubicin), *Cpt2* and *Acot1* were still down-regulated, whereas the other metabolites had recovered (**Figure 5A**, Supplemental Figure 2A).

A similar down-regulation was observed at all time points for gene transcripts encoding glucose cell membrane transporters (*Glut1* and *Glut4*), and the glycolytic enzymes hexokinase 2 and pyruvate dehydrogenase lipoamide kinase isozyme 4 (**Figure 5B**, Supplemental Figure 2B). In vivo ^{18}F-FDG PET studies confirmed a significant reduction in cardiac glucose uptake at all time points examined after the completion of doxorubicin treatment (**Figures 5C and 5D**).

Assessment of the cellular nutrient sensing adenosine monophosphate-activated protein kinase (AMPK) revealed early up-regulation of phosphorylated AMPK (1 week post-doxorubicin), followed by its normalization at later time points (**Figures 5E and 5F**, Supplemental Figures 2C-2E).

DOXORUBICIN ALTERS MITOCHONDRIAL ELECTRON TRANSPORT CHAIN FUNCTION AND ATP PRODUCTION. Mitochondrial function was assessed using high-resolution respirometry of isolated mitochondria. Mitochondrial homogenate preparations were of high quality, as attested by high respiratory control ratios and oxidative phosphorylation (OXPHOS) coupling efficiency ratios (Supplemental Figures 3A and 3B). Mitochondria from doxorubicin-treated mice showed reduced oxygen consumption and low ATP production at all disease stages (**Figures 6A and 6B**). These changes were associated with a reduction in mitochondrial oxygen consumption in the OXPHOS and electron transfer capacity complex I states (**Figures 6C and 6D**). Other respiratory parameters (leak, respiratory control ratio, and OXPHOS coupling efficiency) did not differ between mitochondria from doxorubicin-treated and control mice (**Figure 6E**, Supplemental Figures 3A and 3B).

DOXORUBICIN ALTERS MITOCHONDRIAL DYNAMICS AND QUALITY CONTROL. Transmission electron microscopy of cardiac tissue showed that mitochondrial size and structure remained unaltered 1 week after doxorubicin treatment. Mitochondrial size transiently increased at 9 weeks post-doxorubicin,

FIGURE 3 Cardiac Atrophy, DNA Damage, and Fibrosis

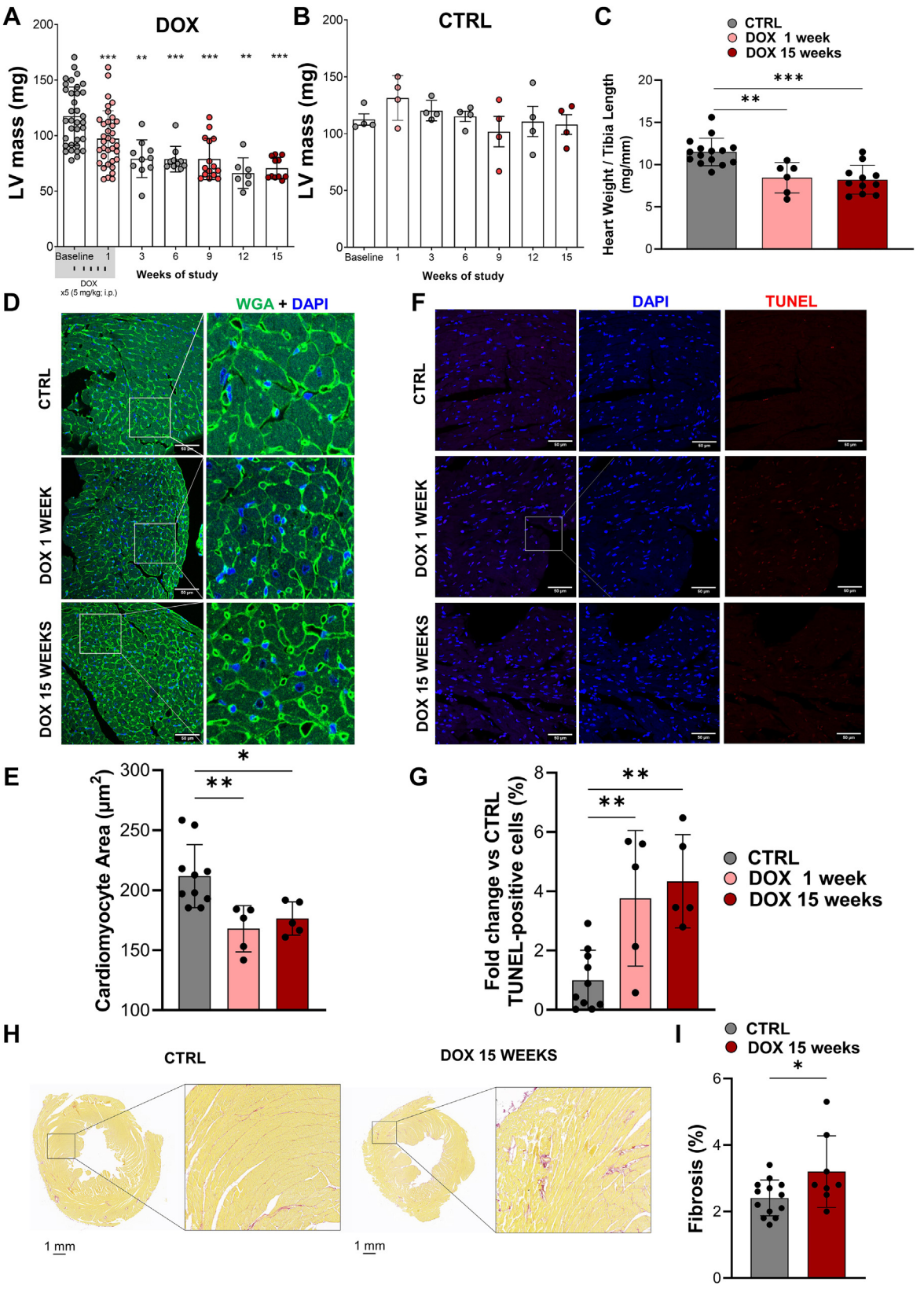

Continued on the next page

FIGURE 4 LVEF Measurement by Echocardiography

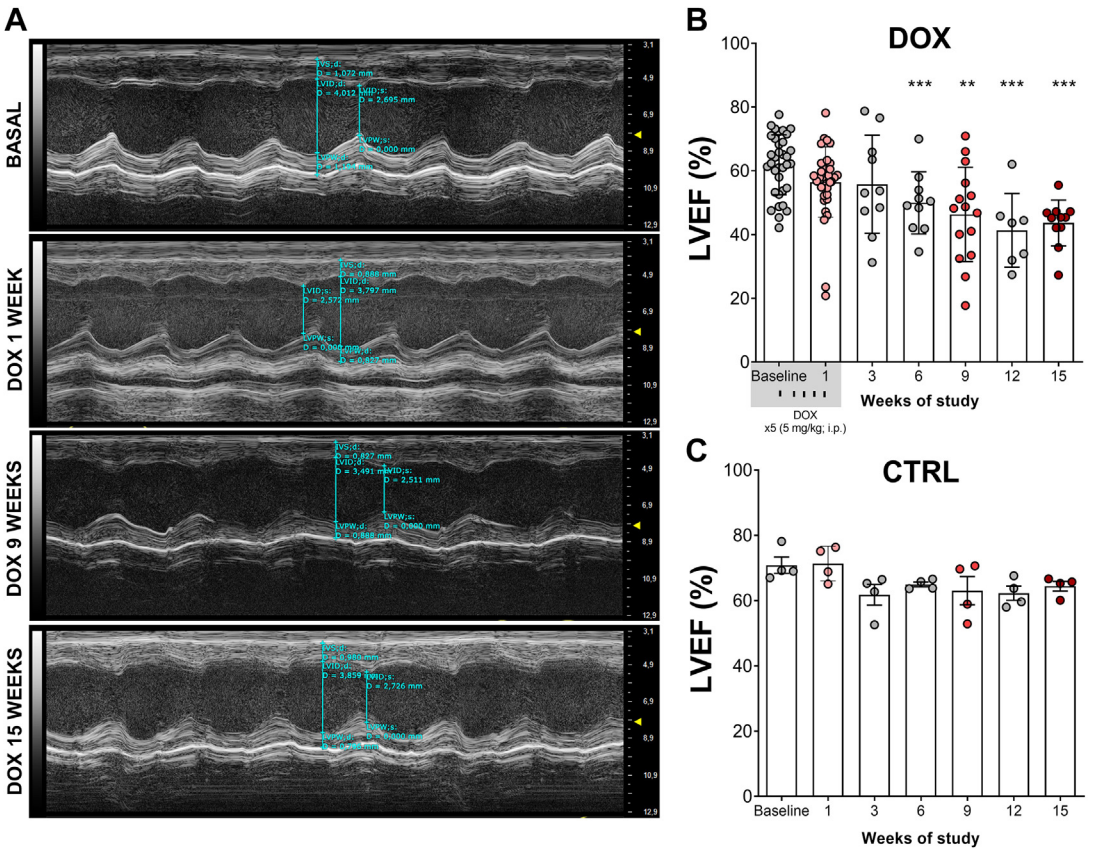

(A) Representative M-mode echocardiographic images. (B,C) LV ejection fraction (LVEF) (%) (n = 4-35). Data are presented as mean ± SD. Data were compared using 1-way repeated-measures ANOVA with Holm-Šídák post hoc test. *$P < 0.05$ and ***$P < 0.001$. Abbreviations as in Figures 1 to 3.

coinciding with a reduction in total mitochondrial number, and this was followed at 15 weeks post-doxorubicin by overt mitochondrial fragmentation, indexed as significantly reduced mitochondrial size (**Figures 7A to 7C**). The increased mitochondrial size in the intermediate disease stage was accompanied by up-regulated expression of the mitochondrial fusion protein optic atrophy type 1 (OPA1), followed by down-regulated expression at 15 weeks (Supplemental Figures 4A and 4B). No significant changes were detected at any disease stage in the expression of dynamin-related protein 1 (DRP1) (Supplemental Figures 4C and 4D).

The mitophagy markers PTEN-induced kinase 1 (PINK1) and E3 ubiquitin-protein ligase parkin (PRKN) were prominently overexpressed at the early disease stage. PINK1 expression subsequently returned to baseline levels, whereas parkin overexpression was

FIGURE 3 Continued

(A,B) Evolution of left ventricular (LV) mass (mg) (n = 4-35) determined from M-mode echocardiographic images. (C) Ratio of heart weight to tibia length 1 and 15 weeks after injections (n = 6-15). (D) Representative photomicrographs of LV myocardial cross sections stained with wheat germ agglutinin (WGA) and 4′,6-diamidino-2-phenylindole (DAPI). Scale bar, 50 μm. (E) Cardiomyocyte cross-sectional area (μm^2) (n = 5-9). (F) Representative photomicrographs of LV myocardial cross sections stained with terminal deoxynucleotidyl transferase dUTP nick-end labeling (TUNEL) assay to assess DNA damage. Scale bar, 50 μm. (G) TUNEL-positive cells (%) (n = 5-10). (H) Representative histologic images illustrating myocardial interstitial fibrosis (Sirius red). Scale bar, 1 mm. (I) Fibrosis (%) (n = 8-13). Data are presented as mean ± SD. Data were compared using 1-way repeated-measures analysis of variance (ANOVA) with Holm-Šídák's post hoc test, ordinary 1-way ANOVA with Dunnett's post hoc test, or unpaired Student's *t*-test. *$P < 0.05$, **$P < 0.01$, and ***$P < 0.001$. Abbreviations as in Figures 1 and 2.

FIGURE 5 Glycolysis and Fatty Acid Metabolism

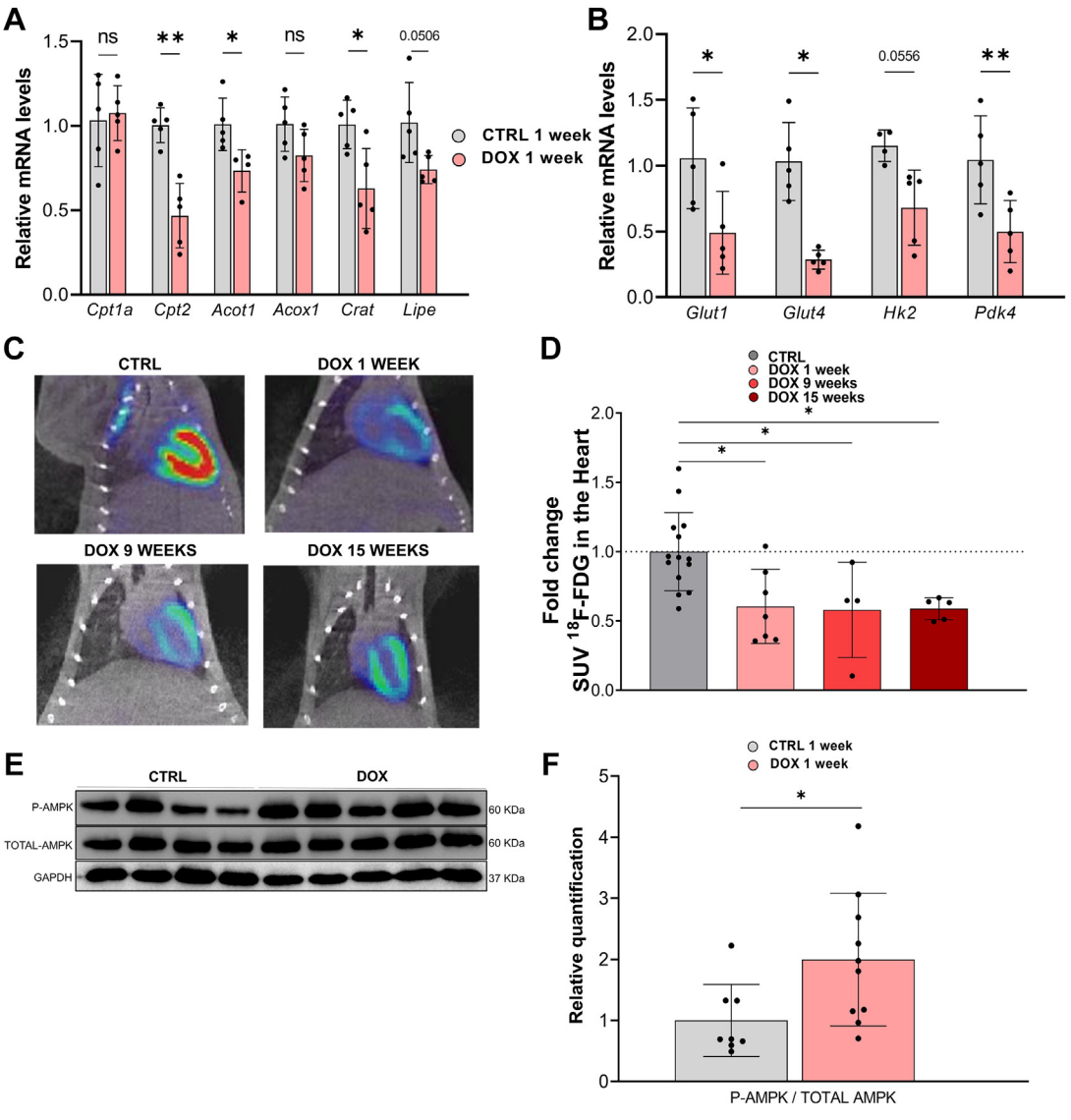

(A,B) Reverse transcriptase quantitative polymerase chain reaction quantification of genes linked to fatty acid metabolism (*Cpt1a*, *Cpt2*, *Acot1*, *Acox1*, *Crat*, and *Lipe*) and glucose metabolism (*Glut1*, *Glut4*, *Hk2*, and *Pdk4*) in cardiac tissue. Gene expression was normalized to *Hprt* messenger RNA (mRNA) (n = 4 or 5). (C) Representative micro-PET/computed tomographic scans. (D) Fold change in the standardized uptake value (SUV) for [^{18}F]-FDG after DOX treatment (n = 4-14). (E,F) Representative western blot and densitometry quantification of phosphorylated adenosine monophosphate-activated protein kinase (P-AMPK) and total AMPK in cardiac tissue 1 week after the final DOX injection (n = 8-10). Glyceraldehyde 3-phosphate dehydrogenase (GAPDH) was used as the loading control. Data are presented as mean ± SD. Data were compared using unpaired Student's *t*-test, Mann-Whitney *U* test, or ordinary 1-way ANOVA with Dunnett's post hoc test. *$P < 0.05$ and **$P < 0.01$. Abbreviations as in Figures 1 to 3.

sustained at week 9 and normalized at week 15 (Figures 7D to 7F). These changes were accompanied by a decrease in mitochondrial DNA content detected at all time points (Figure 7G). Conversely, the key mitochondrial biogenesis protein proliferator-activated receptor gamma coactivator 1-alpha (PGC-1α) was significantly up-regulated 1 week after doxorubicin treatment, regressing to baseline expression levels at subsequent time points (Figures 7H and 7I, Supplemental Figures 4E to 4G).

FIGURE 6 Mitochondrial Function and ATP Production

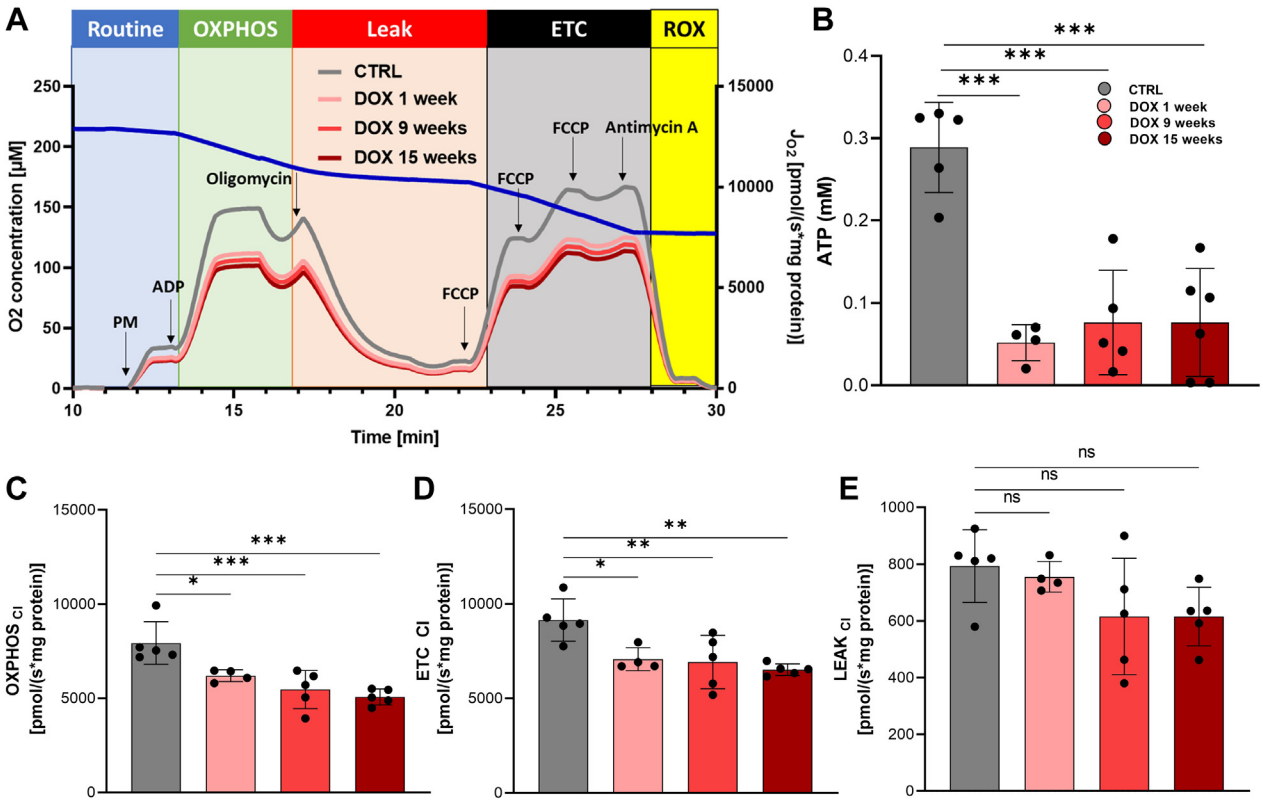

(A) Respirometry traces in mitochondria isolated from hearts. The blue line indicates [O_2]; the gray and red lines indicate O_2 flux per mitochondrial protein (JO_2) in the various conditions. Arrows indicate additions. (B) Mitochondrial adenosine triphosphate (ATP) production at the indicated time points (mM). (C) $OXPHOS_{CI}$. (D) ETC_{CI}. (E) $Leak_{CI}$. Data are presented as mean ± SD. Data were compared using ordinary 1-way ANOVA with Dunnett's post hoc test. *$P < 0.05$, **$P < 0.01$, and ***$P < 0.001$. CI = complex I; ETC = electron transfer capacity; FCCP = carbonyl cyanide-p-trifluoromethoxyphenylhydrazone; OXPHOS = oxidative phosphorylation; PM = pyruvate-malate; ROX = residual oxygen consumption; other abbreviations as in Figures 1 to 3.

DISCUSSION

In this report we present the first longitudinal analysis of temporal cardiac changes occurring during the development of AIC in mice. Our analysis encompasses in vivo cardiac imaging and ex vivo analysis at the early (before any functional impact), intermediate, and late stages of modeled AIC, revealing comprehensive details of anatomical, metabolic, and molecular changes, with particular focus on the central role of mitochondrial damage. Our results show that doxorubicin-induced cardiac functional impairment in mice is preceded at the early disease stage by cardiac atrophy, including cardiomyocyte shrinkage. Early cardiac atrophy was associated with a marked reduction in global cardiac metabolism, affecting both the FA oxidation and the glycolysis pathways and parallel by a marked decrease in ATP production. Early AIC was further characterized by transient up-regulation of the nutrient sensor AMPK, followed by normalization of expression at the intermediate and advanced disease stages. Up-regulated mitophagy in early disease was associated with preserved mitochondrial structure, but a decline in mitophagy at subsequent stages was associated with pronounced mitochondrial fragmentation. The longitudinal assessment of these dynamic processes serves to identify potential targets for therapies aimed at preventing the development of AIC (**Central Illustration**).

MOUSE MODELS OF AIC. Despite the abundant literature on AIC, there is still no consensus on an experimental model of the disease, and the diversity of doxorubicin treatment regimens used limits comparison and reproducibility among studies. Published mouse models of doxorubicin-induced cardiotoxicity include acute (single) and chronic (serial) administrations. In acute models, mice receive a very high

FIGURE 7 Mitochondrial Dynamics

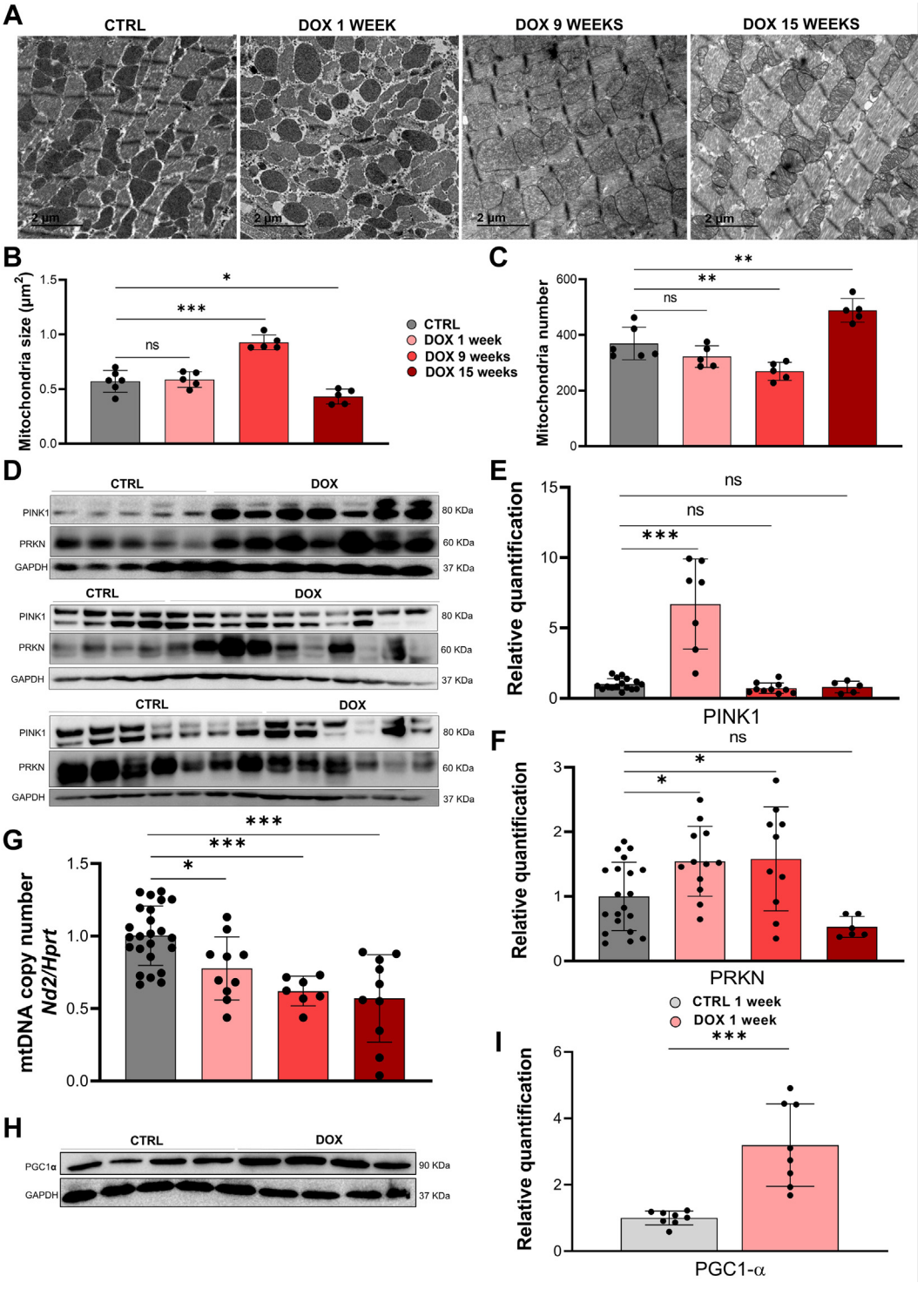

(A) Representative transmission electron microscopic images of cardiac tissue. Scale bar, 2 µm. (B) Mitochondrial size (μm^2) (n = 5). (C) Mitochondrial number (n = 5). (D,E) Representative western blot and (E,F) densitometric quantification of the expression of PTEN-induced kinase 1 (PINK1) (n = 5-16) and E3 ubiquitin-protein ligase parkin (PRKN) (n = 6-20). (G) Mitochondrial DNA (mtDNA) copy number measured as the ratio between *Nd2* (mitochondrial gene) and *Hprt* (nuclear gene) in cardiac tissue (n = 7-24). (H,I) Western blot and densitometry quantification of proliferator-activated receptor gamma coactivator 1-alpha (PGC-1α) at 1 week after DOX treatment (n = 8). GAPDH was used as a loading control. Data are presented as mean ± SD. Data were compared using unpaired Student's *t*-test or ordinary 1-way ANOVA with Dunnett's post hoc test. *$P < 0.05$, **$P < 0.01$, and ***$P < 0.001$. Abbreviations as in Figures 1 to 3 and 5.

CENTRAL ILLUSTRATION **Longitudinal Assessment of AIC and Novel Therapeutic Targets**

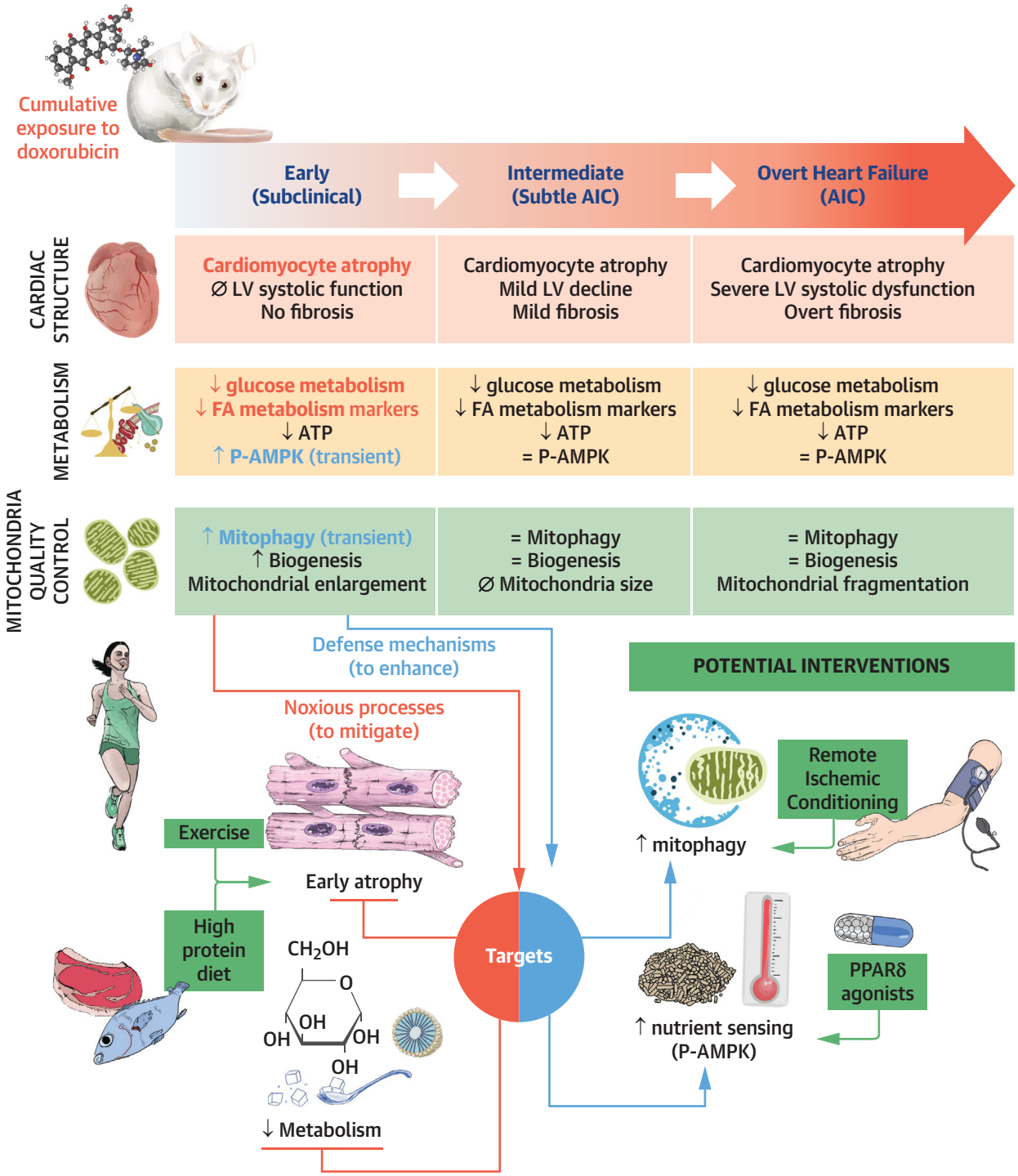

Díaz-Guerra A, et al. J Am Coll Cardiol CardioOnc. 2024;6(2):217–232.

Principal effects of cumulative exposure to doxorubicin in mice on cardiac structure, metabolism, and mitochondria quality control. Timeline extends from subclinical to intermediate to overt heart failure stages: 1 to 15 weeks after doxorubicin treatment. Potential interventions against cardiotoxicity include enhancing defense mechanisms and mitigating the noxious processes activated during time of study. The early atrophy and decrease in FA metabolism may be alleviated by exercise and high-protein diets, the transient increase in mitophagy by remote ischemic conditioning, and increase in nutrient sensing by peroxisome-proliferator-associated receptor δ (PPARδ) agonists. AIC = anthracycline-induced cardiotoxicity; ATP = adenosine triphosphate; FA = fatty acids; LV = left ventricular; mtDNA = mitochondrial DNA; P-AMPK = phosphorylated adenosine monophosphate-activated protein kinase.

single dose of doxorubicin that rapidly damages the heart, leading to early high mortality and limiting the possibility of longitudinal evaluation.[13] In our study, we used a chronic model based on serial administration of doxorubicin, which induced slowly progressive cardiac dysfunction that more closely resembles the long-term clinical scenario. In a previous study using a similar approach and achieving a similar cumulative dose (20-25 mg/kg), cardiac function was analyzed at only a single time point.[14] In contrast, our study provides serial long-term analysis of cardiac function. The longitudinal echocardiographic assessment revealed that LV systolic dysfunction develops progressively after doxorubicin exposure and is preceded by several processes, including cardiac atrophy. These processes might represent potential therapeutic targets.

CARDIAC ATROPHY PRECEDES SYSTOLIC DYSFUNCTION IN AIC. The early disease stage after doxorubicin treatment, when cardiac function was still preserved, was characterized by reductions in LV mass detected by echocardiography, heart weight, and cardiomyocyte area. A decrease in cardiac mass after doxorubicin exposure has been reported previously in clinical trials[15,16] and in mouse models.[17] Although the mechanism of cardiomyocyte atrophy after doxorubicin exposure is poorly understood, there is evidence that it could be mediated by activation of cyclin-dependent kinase 2 (CDK2)-dependent forkhead box protein O1 (FOXO1).[18] It is known that DNA damage can cause cardiomyocyte atrophy. In this regard, we found a significant increase of TUNEL-positive cardiomyocytes (**Figures 3F and 3G**). Given that BCL2/BAX ratios were not increased in doxorubicin-treated mice (data not shown), we speculate that the TUNEL signal may come from cytoplasmic DNA damage that does not result in apoptosis. These findings suggest that interventions targeting early doxorubicin-induced cardiomyocyte atrophy could represent a therapeutic benefit in AIC. One possible approach to alleviating cardiac atrophy is increased physical activity,[15] and benefits might also be obtained with specific nutritional approaches such as high-protein or high-calorie diets, as caloric restriction is known to induce LV atrophy.[19] The progression in our model from early cardiac atrophy to deteriorating cardiac function at the intermediate and advanced AIC stages parallels observations in anthracycline-treated cancer survivors.[20]

REDUCTION OF GLOBAL CARDIAC METABOLISM EARLY IN THE COURSE OF AIC. Cardiac metabolism showed a marked decline from the early stage of AIC, consisting of a general decrease in FA and glucose metabolism. This cardiac hypometabolism could be a consequence of ultrastructural damage in the inner mitochondrial membrane caused by doxorubicin binding to cardiolipin,[7] disrupting the transporter activities of proteins involved in FA oxidation, such as Cpt2, as described in doxorubicin-treated rats.[21] The high affinity of doxorubicin for the mitochondrial inner membrane can also interrupt the enzymatic activities of complexes I, II, and IV, resulting in blockade of mitochondrial FA oxidation and decreased ATP production.[22] This was evidenced in the decreased mitochondrial respiration in doxorubicin-treated mice and the associated decrease in mitochondrial ATP production. Mitochondrial dysfunction in our model is also evidenced by the reduced mitochondrial DNA content in doxorubicin-treated mice at all time points studied. Mitochondrial DNA damage has also been reported as a consequence of doxorubicin intercalation into mitochondrial DNA, resulting in iron accumulation.[23]

Reduced cardiac glucose metabolism was evidenced by the early down-regulation of the cell membrane glucose transporters Glut1 and Glut4 in cardiomyocytes of doxorubicin-treated mice. Cardiomyocyte Glut4 down-regulation in doxorubicin-treated rats has been proposed to be secondary to cell membrane perturbation after doxorubicin intercalation.[24,25] Impaired glucose import can also be a consequence of doxorubicin-induced insulin resistance;[24] however, this is unlikely to be the case in our model, as insulin handling was unaffected in the doxorubicin-treated mice (Supplemental Figure 1E). Thus, the decreases in Glut1 and Glut4 in our study appear to be related to structural cell membrane defects. The decreased glycolysis in our AIC model is consistent with previous mouse and cell-line studies showing doxorubicin-induced decreases in adipose tissue glucose uptake,[12] plasma glucose and lactate, and the glycolytic enzyme hexokinase 2.[26] The down-regulation of glucose importers correlated with a reduced in vivo cardiac uptake of FDG in the doxorubicin-treated mice. Although these results are in agreement with some previous studies showing reduced cardiac glucose uptake in rats exposed to doxorubicin,[27] other groups have reported that doxorubicin exposure increases cardiac FDG uptake.[11] This discrepancy might be attributable to differences in FDG PET timing, acute vs chronic doxorubicin injection regimes, or the mechanisms induced by intravenous vs intraperitoneal doxorubicin administration. Another possible explanation is that the effect of AIC on cardiac glucose uptake may vary between species or even mouse strains.

The transient up-regulation of the energy-stress sensor AMPK[28] in cardiomyocytes early after doxorubicin treatment may be a defense response to the low availability of metabolic substrates, given that the master regulator AMPK promotes glucose and FA uptake.[29] The early AMPK activation was likely responsible for the up-regulation of mitochondrial biogenesis (PGC-1α) and mitophagy (PINK1/parkin) pathways, both of which are regulated by AMPK.[30] However, despite AMPK signaling activation, the doxorubicin-treated mice were unable to increase oxidative catabolism of either glucose or FAs, likely because of irreversible doxorubicin-induced damage to the inner mitochondrial membrane or intestinal injury. AMPK signaling is an essential regulator of mitochondrial homeostasis and energy metabolism, and the search for AMPK-targeting strategies has been a central goal of AIC research.[31] The suggestion from our findings that AMPK activation also contributes to mitochondrial reprogramming after doxorubicin insult may help identify candidate molecules for new therapeutic strategies in AIC.

General activation of cardiac metabolism represents an attractive possible therapeutic approach to AIC. Dietary nutrients were recently shown to ameliorate chemotherapy-induced LV dysfunction and to protect the cardiovascular system both in animals (mouse and rat) and in patients with cancer.[32] Furthermore, amino acid–enriched diets have been found to promote cell survival in doxorubicin-treated mice,[33] demonstrating the cardioprotective role of diet against AIC. Some metabolic activators, such as metformin, dietary restriction, and exercise, can activate AMPK and could have a favorable anti-cardiotoxicity effect.[34] Another potential target is the AMPK substrate peroxisome proliferator–associated receptor δ (PPARδ), a nuclear receptor transcription factor that controls lipid metabolism and inflammation.[35] PPARδ agonists have attracted attention for their potential in cancer therapy[36] and have been proposed as cardioprotective agents that prevent cardiomyocyte apoptosis after doxorubicin exposure.[37]

MITOCHONDRIAL DYNAMICS AND QUALITY CONTROL DURING AIC. The defective mitochondrial ATP production we detected from the early stage of AIC is in line with previous findings.[38] Defective mitochondria are usually selectively eliminated through mitophagy to prevent the accumulation of toxic products and avoid fusion of damaged mitochondria with the healthy network.[39] This quality control mechanism is critical to maintaining a healthy mitochondrial mass during stress. When this mechanism is overwhelmed, cardiomyocyte dysfunction occurs.[40] Doxorubicin exposure in our model induced early (transient) up-regulation of the mitophagy PINK1/parkin pathway, which has been previously linked to the protective removal of dysfunctional mitochondria during doxorubicin insults.[41] In addition to its role in mitophagy, parkin has been reported to enhance mitochondrial activity via interaction with the master regulator of mitochondrial biogenesis, PGC-1α.[42] PGC-1α was also up-regulated early after doxorubicin treatment in our model, and we propose that the early up-regulation of this quality control machinery is a defense mechanism that helps preserve cardiac function in the early phase of AIC. The up-regulation of mitophagy and mitochondrial biogenesis presents another attractive target for early intervention in AIC. Mitophagy was also identified as an early feature of AIC in a previous study in our laboratory in a pig model.[43] In the same pig AIC model, we previously reported that remote ischemic conditioning, an intervention able to increase mitophagy,[44] prevents AIC.[45]

In addition to mitophagy and biogenesis, mitochondria can enhance cell survival through dynamic transitions of fusion and fission. Activation of mitochondrial fusion at the early and intermediate AIC stages in our model is suggested by the overexpression of the fusion marker OPA1 and the increased mitochondrial size on transmission electron microscopy. Mitochondrial fusion has the effect of diluting injured mitochondrial DNA, which has been shown to rescue cardiac dysfunction in doxorubicin-treated mice.[10] In our model, the increased mitochondrial fusion and enhanced mitophagy likely mitigated the impaired respiration capacity observed in isolated mitochondria at all time points studied, allowing transient maintenance of cardiac function until the system was overwhelmed. This hypothesis is supported by the fact that overt cardiac systolic dysfunction correlates with the exhaustion of mitophagy and the onset of mitochondrial fragmentation.[46] Doxorubicin-associated fission (occurring late in AIC) has been described in other studies in mice[47] and pigs.[45] Inhibition of mitochondrial fission could thus offer another therapeutic strategy in AIC and has been shown to prevent cardiac dysfunction in ischemia and reperfusion injury.[48]

SEX-BASED DIFFERENCES IN ANTHRACYCLINE CARDIOTOXICITY. We focused only on male mice in this study. The influence of sex on anthracycline-induced HF remains a subject of debate.[49] Although the precise impact of sex in this context is not definitively established, there is a growing hypothesis suggesting a role for female sex hormones in protecting against doxorubicin-induced cardiotoxicity. This hypothesis posits that prepubescent girls and

postmenopausal women, lacking the protective effects conferred by female hormones, might exhibit heightened susceptibility to anthracycline-induced heart complications. This proposition aligns with observations noting a potentially higher vulnerability in these demographic groups because of the absence of female hormones. Therefore, it is theorized that adult women, benefiting from the presence of these hormones, may have a certain degree of cardioprotection against AIC.[50] Additionally, another study delved deeper into this notion of estrogen's protective role against chronic doxorubicin treatment within the heart. Those investigators proposed that estrogen may contribute to the preservation of myofilament function, ultimately mitigating oxidative modifications linked to AIC.[51] These varying perspectives underscore the complexity of the interplay between sex hormones, particularly estrogen, and the development of anthracycline-induced heart complications. In our investigation, a preliminary study was undertaken to validate the therapeutic targets identified in the early stages of AIC in female CD1 mice (Supplemental Figure 5). Our findings indicate that cardiac atrophy and hypometabolism manifest in both sexes at early time points, specifically 1 week after anthracycline administration. Nevertheless, the comprehensive delineation of sex-specific distinctions subsequent to doxorubicin exposure in CD1 strain necessitates additional experimentation. Further exploration is warranted to elucidate the precise mechanisms underlying these observations and to potentially leverage this understanding for more targeted approaches in mitigating cardiotoxic effects in susceptible populations.

STUDY LIMITATIONS. The AIC model presented here has some differences from the clinical scenario. Some of the biological processes affected may differ between mice and humans. The lack of a tumoral background in the model can overlook the impact of the interplay among cancer, chemotherapy, and cardiovascular function. This limitation is at the same time an advantage, as this nontumor model allows study the specific effects of anthracyclines in an environment without noise.

CONCLUSIONS

This study provides the first comprehensive timeline of cardiac anatomical, functional, and molecular changes occurring during the progression of AIC in mice. Our results identify early events after doxorubicin exposure with potential as therapeutic targets, including cardiac atrophy, mitophagy, and the activation of nutrient-sensing pathways. Future validation of these targets will help in the development of interventions to prevent AIC progression before the appearance of overt cardiac functional impairment.

ACKNOWLEDGMENTS Simon Bartlett (Centro Nacional de Investigaciones Cardiovasculares) provided English editing. The authors thank Santiago Rodriguez-Colilla for help with animal care and Francisco Urbano for help with transmission electron microscopy.

FUNDING SUPPORT AND AUTHOR DISCLOSURES

Dr Ibáñez is supported by the European Commission (grants ERC-CoG 819775 and H2020-HEALTH 945118), the Spanish Ministry of Science, Innovation and Universities (grant PID2022-140176OB-I00), and Comunidad de Madrid through the Red Madrileña de Nanomedicina en Imagen Molecular (grant P2022/BMD-7403 RENIM-CM). Dr Díaz-Guerra's PhD fellowship is funded by the Spanish Association Against Cancer. Dr Oliver is a Ramón y Cajal fellow (grant RYC2020-028884-I) funded by MCIN/AEI/10.13039/501100011033 and by "ESF Investing in Your Future." Centro Nacional de Investigaciones Cardiovasculares is supported by Instituto de Salud Carlos III, Ministerio de Ciencia e Innovación, and the Pro CNIC Foundation and is a Severo Ochoa Center of Excellence (grant CEX2020-001041-S funded by MICIN/AEI/10.13039/501100011033). The authors have reported that they have no relationships relevant to the contents of this paper to disclose.

ADDRESS FOR CORRESPONDENCE: Dr Borja Ibanez, Translational Laboratory for Cardiovascular Imaging and Therapy, Centro Nacional de Investigaciones Cardiovasculares Carlos III, and IIS-Fundación Jiménez Díaz University Hospital, c/ Melchor Fernandez Almagro, 3, 28029 Madrid, Spain. E-mail: bibanez@cnic.es.

PERSPECTIVES

COMPETENCY IN MEDICAL KNOWLEDGE/ COMPETENCY IN PATIENT CARE: The alterations induced by exposure to doxorubicin that lead to cardiotoxicity are dynamic, and some processes might be important at some stages and not at others. Early changes occurring in the myocardium before any functional impact, such as cardiac atrophy, transient up-regulation of nutrient-sensing pathways, and transient enhanced mitophagy, present potential novel candidate therapeutic targets for the prevention of overt AIC.

TRANSLATIONAL OUTLOOK: Validation of the cardioprotection potential of our identified novel therapeutic targets in animal models are important to lay the foundation for future clinical trials.

REFERENCES

1. Omland T, Heck SL, Gulati G. The role of cardioprotection in cancer therapy cardiotoxicity: *JACC: CardioOncology* state-of-the-art review. *J Am Coll Cardiol CardioOnc*. 2022;4:19–37.

2. Lyon AR, Lopez-Fernandez T, Couch LS, et al. 2022 ESC guidelines on cardio-oncology developed in collaboration with the European Hematology Association (EHA), the European Society for Therapeutic Radiology and Oncology (ESTRO) and the International Cardio-Oncology Society (IC-OS). *Eur Heart J*. 2022;43:4229–4361.

3. Lopez-Sendon J, Alvarez-Ortega C, Zamora Aunon P, et al. Classification, prevalence, and outcomes of anticancer therapy-induced cardiotoxicity: the CARDIOTOX registry. *Eur Heart J*. 2020;41:1720–1729.

4. Demissei BG, Vedage NA, Hubbard RA, et al. Longitudinal right ventricular systolic function changes in breast cancer patients treated with cardiotoxic cancer therapy. *J Am Coll Cardiol CardioOnc*. 2022;4:552–554.

5. Ibanez B, Moreno-Arciniegas A. The quest for an early marker of anthracycline-induced cardiotoxicity. *J Am Coll Cardiol Basic Trans Science*. 2022;7:11–13.

6. Henriksen PA, Rankin S, Lang NN. Cardioprotection in patients at high risk of anthracycline-induced cardiotoxicity: *JACC: CardioOncology* primer. *J Am Coll Cardiol CardioOnc*. 2023;5:292–297.

7. Murabito A, Hirsch E, Ghigo A. Mechanisms of anthracycline-induced cardiotoxicity: is mitochondrial dysfunction the answer? *Front Cardiovasc Med*. 2020;7:35.

8. Gorini S, De Angelis A, Berrino L, Malara N, Rosano G, Ferraro E. Corrigendum to "Chemotherapeutic drugs and mitochondrial dysfunction: focus on doxorubicin, trastuzumab, and sunitinib." *Oxid Med Cell Longev*. 2019;2019:9601435.

9. Schirone L, D'Ambrosio L, Forte M, et al. Mitochondria and doxorubicin-induced cardiomyopathy: a complex interplay. *Cells*. 2022;11(13):2000.

10. Abdullah CS, Alam S, Aishwarya R, et al. Doxorubicin-induced cardiomyopathy associated with inhibition of autophagic degradation process and defects in mitochondrial respiration. *Sci Rep*. 2019;9:2002.

11. Cordoba-Adaya JC, Oros-Pantoja R, Torres-Garcia E, et al. Evaluation of doxorubicin-induced early multi-organ toxicity in male CD1 mice by biodistribution of ^{18}F-FDG and ^{67}Ga-citrate. Pilot study. *Toxicol Mech Methods*. 2021;31:546–558.

12. Biondo LA, Batatinha HA, Souza CO, et al. Metformin mitigates fibrosis and glucose intolerance induced by doxorubicin in subcutaneous adipose tissue. *Front Pharmacol*. 2018;9:452.

13. An L, Wuri J, Zheng Z, Li W, Yan T. Microbiota modulate doxorubicin induced cardiotoxicity. *Eur J Pharm Sci*. 2021;166:105977.

14. Li L, Li J, Wang Q, et al. Shenmai injection protects against doxorubicin-induced cardiotoxicity via maintaining mitochondrial homeostasis. *Front Pharmacol*. 2020;11:815.

15. Chen DS, Yan J, Yang PZ. Cardiomyocyte atrophy, an underestimated contributor in doxorubicin-induced cardiotoxicity. *Front Cardiovasc Med*. 2022;9:812578.

16. Ferreira de Souza T, Quinaglia ACST, Osorio Costa F, et al. Anthracycline therapy is associated with cardiomyocyte atrophy and preclinical manifestations of heart disease. *J Am Coll Cardiol Img*. 2018;11:1045–1055.

17. Rasanen M, Degerman J, Nissinen TA, et al. VEGF-B gene therapy inhibits doxorubicin-induced cardiotoxicity by endothelial protection. *Proc Natl Acad Sci U S A*. 2016;113:13144–13149.

18. Xia P, Chen J, Liu Y, Fletcher M, Jensen BC, Cheng Z. Doxorubicin induces cardiomyocyte apoptosis and atrophy through cyclin-dependent kinase 2-mediated activation of forkhead box O1. *J Biol Chem*. 2020;295:4265–4276.

19. Gruber C, Nink N, Nikam S, et al. Myocardial remodelling in left ventricular atrophy induced by caloric restriction. *J Anat*. 2012;220:179–185.

20. Nousiainen T, Jantunen E, Vanninen E, Hartikainen J. Early decline in left ventricular ejection fraction predicts doxorubicin cardiotoxicity in lymphoma patients. *Br J Cancer*. 2002;86:1697–1700.

21. Yoon HR, Hong YM, Boriack RL, Bennett MJ. Effect of L-carnitine supplementation on cardiac carnitine palmitoyltransferase activities and plasma carnitine concentrations in adriamycin-treated rats. *Pediatr Res*. 2003;53:788–792.

22. Wenningmann N, Knapp M, Ande A, Vaidya TR, Ait-Oudhia S. Insights into doxorubicin-induced cardiotoxicity: molecular mechanisms, preventive strategies, and early monitoring. *Mol Pharmacol*. 2019;96:219–232.

23. Abe K, Ikeda M, Ide T, et al. Doxorubicin causes ferroptosis and cardiotoxicity by intercalating into mitochondrial DNA and disrupting Alas1-dependent heme synthesis. *Sci Signal*. 2022;15:eabn8017.

24. de Lima Junior EA, Yamashita AS, Pimentel GD, et al. Doxorubicin caused severe hyperglycaemia and insulin resistance, mediated by inhibition in AMPk signalling in skeletal muscle. *J Cachexia Sarcopenia Muscle*. 2016;7:615–625.

25. Biondo LA, Lima Junior EA, Souza CO, et al. Impact of doxorubicin treatment on the physiological functions of white adipose tissue. *PLoS One*. 2016;11:e0151548.

26. Sharma RI, Welch AE, Schweiger L, Craib S, Smith TA. [F]fluoro-2-deoxy-d-glucose incorporation by mcf-7 breast tumour cells in vitro is modulated by treatment with tamoxifen, doxorubicin, and docetaxel: relationship to chemotherapy-induced changes in ATP content, hexokinase activity, and glucose transport. *Int J Mol Imaging*. 2011;2011:874585.

27. Montaigne D, Marechal X, Baccouch R, et al. Stabilization of mitochondrial membrane potential prevents doxorubicin-induced cardiotoxicity in isolated rat heart. *Toxicol Appl Pharmacol*. 2010;244:300–307.

28. Hardie DG. AMPK—sensing energy while talking to other signaling pathways. *Cell Metab*. 2014;20:939–952.

29. O'Neill HM. AMPK and exercise: glucose uptake and insulin sensitivity. *Diabetes Metab J*. 2013;37:1–21.

30. Hardie DG, Ross FA, Hawley SA. AMPK: a nutrient and energy sensor that maintains energy homeostasis. *Nat Rev Mol Cell Biol*. 2012;13:251–262.

31. Singh M, Nicol AT, DelPozzo J, et al. Demystifying the relationship between metformin, AMPK, and doxorubicin cardiotoxicity. *Front Cardiovasc Med*. 2022;9:839644.

32. Zhang XY, Yang KL, Li Y, et al. Can dietary nutrients prevent cancer chemotherapy-induced cardiotoxicity? An evidence mapping of human studies and animal models. *Front Cardiovasc Med*. 2022;9:921609.

33. Corsetti G, Romano C, Pasini E, Scarabelli T, Chen-Scarabelli C, Dioguardi FS. Essential amino acids-rich diet increases cardiomyocytes protection in doxorubicin-treated mice. *Nutrients*. 2023;15(10):2287.

34. Timm KN, Tyler DJ. The role of AMPK activation for cardioprotection in doxorubicin-induced cardiotoxicity. *Cardiovasc Drugs Ther*. 2020;34:255–269.

35. Palomer X, Barroso E, Pizarro-Delgado J, et al. PPARbeta/delta: a key therapeutic target in metabolic disorders. *Int J Mol Sci*. 2018;19(3):913.

36. Wagner N, Wagner KD. PPAR beta/delta and the hallmarks of cancer. *Cells*. 2020;9(5):1133.

37. Altieri P, Spallarossa P, Barisione C, et al. Inhibition of doxorubicin-induced senescence by PPARdelta activation agonists in cardiac muscle cells: cooperation between PPARdelta and Bcl6. *PLoS One*. 2012;7:e46126.

38. Pointon AV, Walker TM, Phillips KM, et al. Doxorubicin in vivo rapidly alters expression and translation of myocardial electron transport chain genes, leads to ATP loss and caspase 3 activation. *PLoS One*. 2010;5:e12733.

39. Youle RJ, Narendra DP. Mechanisms of mitophagy. *Nat Rev Mol Cell Biol*. 2011;12:9–14.

40. Wu Y, Jiang T, Hua J, et al. PINK1/parkin-mediated mitophagy in cardiovascular disease: From pathogenesis to novel therapy. *Int J Cardiol*. 2022;361:61–69.

41. Zhou JC, Jin CC, Wei XL, et al. Mesaconine alleviates doxorubicin-triggered cardiotoxicity and heart failure by activating PINK1-dependent cardiac mitophagy. *Front Pharmacol*. 2023;14:1118017.

42. Zheng L, Bernard-Marissal N, Moullan N, et al. Parkin functionally interacts with PGC-1alpha to preserve mitochondria and protect dopaminergic neurons. *Hum Mol Genet*. 2017;26:582–598.

43. Galan-Arriola C, Lobo M, Vilchez-Tschischke JP, et al. Serial magnetic resonance

imaging to identify early stages of anthracycline-induced cardiotoxicity. *J Am Coll Cardiol*. 2019;73:779–791.

44. Huang C, Andres AM, Ratliff EP, Hernandez G, Lee P, Gottlieb RA. Preconditioning involves selective mitophagy mediated by parkin and p62/SQSTM1. *PLoS One*. 2011;6:e20975.

45. Galan-Arriola C, Villena-Gutierrez R, Higuero-Verdejo MI, et al. Remote ischaemic preconditioning ameliorates anthracycline-induced cardiotoxicity and preserves mitochondrial integrity. *Cardiovasc Res*. 2021;117:1132–1143.

46. Wu J, Chen H, Qin J, et al. Baicalin improves cardiac outcome and survival by suppressing Drp1-mediated mitochondrial fission after cardiac arrest-induced myocardial damage. *Oxid Med Cell Longev*. 2021;2021:8865762.

47. Liang X, Wang S, Wang L, Ceylan AF, Ren J, Zhang Y. Mitophagy inhibitor liensinine suppresses doxorubicin-induced cardiotoxicity through inhibition of Drp1-mediated maladaptive mitochondrial fission. *Pharmacol Res*. 2020;157:104846.

48. Cooper HA, Eguchi S. Inhibition of mitochondrial fission as a novel therapeutic strategy to reduce mortality upon myocardial infarction. *Clin Sci (Lond)*. 2018;132:2163–2167.

49. Diaz ANR, Hurtado GP, Manzano AAA, et al. Sex differences in the development of anthracycline-associated heart failure. *J Card Fail*. Published online November 10, 2023. https://doi.org/10.1016/j.cardfail.2023.10.477.

50. Cadeddu Dessalvi C, Pepe A, Penna C, et al. Sex differences in anthracycline-induced cardiotoxicity: the benefits of estrogens. *Heart Fail Rev*. 2019;24:915–925.

51. Rattanasopa C, Kirk JA, Bupha-Intr T, Papadaki M, de Tombe PP, Wattanapermpool J. Estrogen but not testosterone preserves myofilament function from doxorubicin-induced cardiotoxicity by reducing oxidative modifications. *Am J Physiol Heart Circ Physiol*. 2019;316:H360–H370.

KEY WORDS **anthracyclines, cancer, cardio-oncology, cardiotoxicity, doxorubicin, mitochondria**

APPENDIX **For supplemental methods, figures, and a supplemental table, please see the online version of this paper.**